PHYSICAL REVIEW B **82**, 081411(R) (2010)

Impurity-assisted nanoscale localization of plasmonic excitations in graphene

Rodrigo A. Muniz,[1,*] Hari P. Dahal,[2] A. V. Balatsky,[2,†] and Stephan Haas[1]
[1]*Department of Physics and Astronomy, University of Southern California, Los Angeles, California 90089-0484, USA*
[2]*Theoretical Division and Center for Integrated Nanotechnology, Los Alamos National Laboratory, Los Alamos, New Mexico 87545, USA*
(Received 28 July 2010; published 20 August 2010)

A nonlocal quantum-mechanical model is employed to compute plasmonic excitations of graphene in the presence of an impurity potential. A full diagonalization of the polarization operator is performed, allowing the extraction of all its poles. It is demonstrated that impurities induce the formation of nanoscale localized plasmonic modes. It is also shown that the chemical potential and impurity strength can be tuned to control target features of the localized modes, making graphene an intrinsic plasmonic material. These predictions can be tested by scanning tunneling microscopy experiments.

DOI: 10.1103/PhysRevB.82.081411 PACS number(s): 73.22.−f, 71.45.Gm, 73.20.Mf

I. INTRODUCTION

Localized plasmonic excitations have the ability of squeezing light beyond the diffraction limit. This property has been extensively employed in enhancement and photonics applications.[1] Therefore, there is obvious interest in finding structures presenting these kind of excitations.

Graphene is a one atom thick layer of carbon atoms arranged in a honeycomb lattice. Due to its thin crystal structure it is a promising material for a wide range of nanotechnological applications.[2] *Ab initio* calculations have shown that graphene is a gapless semiconductor, for which the valence and conduction bands meet at the Fermi energy. At this point the energy dispersion of the quasiparticle excitations has been found to be linear.[3] Experimentally, the system can be tuned into a metallic regime by adjusting the chemical potential using a gate voltage.[4] Due to these unique properties there is considerable current interest in the electronic properties of this material.[5–9]

Recent scanning tunneling microscopy (STM) experiments have shown that graphene is intrinsically disordered.[10] In order to determine its technological usefulness, it is therefore important to understand the effects of disorder on its electronic properties. Much recent research has focused on the effects of impurities on the ground-state properties of graphene.[11–15] There are however some recent studies of the plasmonic modes in graphene using the linearized band structure[16–19] and a full tight-binding band-structure calculation.[20] The effects of a fully gapped band[21] and doping[22] have also been explored. But none of these works considered localized plasmons. A more recent work showed however that localized states can have a significant effect on tunneling.

In this Rapid Communication, we examine the consequences of the presence of impurities on the plasmonic modes in graphene. Our main focus is to obtain and control localized plasmons. The analysis of these features requires the determination of their spatial profile, which is provided in this study. Our results show that even simple kinds of impurities in graphene generate many localized plasmonic modes which makes graphene an intrinsic nanoplasmonic material.

II. MODEL

The classical computation of plasmonic modes through the Mie theory breaks down for nanostructures with features smaller than some few nanometers. There are two reasons:[23] the dielectric function is not uniform throughout the sample which was addressed by a recent work[24] and the system requires a quantum-mechanical description.

Recently, a nonlocal self-consistent quantum-mechanical approach was developed, which accounts for the nonlocality of the dielectric-response function.[25] Using this technique, the identification of plasmons was accomplished by scanning the frequencies of the modes with strongest induced fields. However, it does not provide full information of all plasmon excitations supported by the system. In this contribution, we generalize this approach. The polarization operator is diagonalized providing all its poles. Thus complete information of the plasmon excitations is obtained, including the local spectral densities of states. A key quantity for comparison with STM experiments. Therefore this method is also useful for understanding basic properties of graphene from a more fundamental point of view.

We model the electronic structure of graphene using a one-band tight-binding Hamiltonian,

$$H_0 = -t\sum_{\langle a,b\rangle}(c_a^\dagger c_b + c_b^\dagger c_a) + \sum_a U_a c_a^\dagger c_a - \mu\sum_a c_a^\dagger c_a, \quad (1)$$

where $t=2.7$ eV is the hopping parameter and μ is the chemical potential. U_0 is the magnitude of the impurity potential, $\mathbf{x}_0$ corresponds to its location, and σ denotes its spatial spread. U_a is then the impurity potential felt at the other sites $\mathbf{x}_a \neq \mathbf{x}_0$, parametrized by $U_a = U_0 \exp(\frac{-|\mathbf{x}_a-\mathbf{x}_0|^2}{2\sigma^2})$. In this Rapid Communication, the range of the impurity potential σ will be only few lattice sites. H_0 is diagonalized numerically, providing the eigenstates $|\Psi_\alpha^0\rangle$ and eigenvalues E_α^0.

The direct Coulomb interaction is considered as a perturbation,

$$H = H_0 + V = H_0 + \sum_{abmn} V_{abmn} c_a^\dagger c_b^\dagger c_m c_n \quad (2)$$

with

$$V_{abmn} = \frac{e^2}{2}\int d\mathbf{x}\int d\mathbf{x}' \frac{\varphi_a^*(\mathbf{x})\varphi_b^*(\mathbf{x}')\varphi_m(\mathbf{x}')\varphi_n(\mathbf{x})}{|\mathbf{x}-\mathbf{x}'|}, \quad (3)$$

where $\varphi_j(\mathbf{x})$ is the p_z orbital at site j. In the lattice basis the induced charge is given by

$$\delta\rho(\mathbf{x}) = \sum_{ab} \varphi_a^*(\mathbf{x})\delta\rho_{ab}\varphi_b(\mathbf{x}) = \sum_b \varphi_b^*(\mathbf{x})\delta\rho_{bb}\varphi_b(\mathbf{x}).$$

Here the overlap of p_z orbitals at different sites is neglected $\varphi_a^*(\mathbf{x})\varphi_b(\mathbf{x}) = \delta_{ab}\varphi_b^*(\mathbf{x})\varphi_b(\mathbf{x})$. The linear-response charge equation on this basis is

$$\delta\rho_{ab}(\omega) = \sum_{mn} \Pi_{ab,mn}(\omega)\phi_{mn}^{Ext}(\omega). \tag{4}$$

Within the random-phase approximation (RPA), the polarization operator is then obtained via $\Pi(\omega) = \Pi^0(\omega)[1 - V\Pi^0(\omega)]^{-1}$, where $\Pi^0(\omega)$ is the polarization operator of the noninteracting system. In the basis of eigenstates $|\Psi_\alpha^0\rangle$, $\Pi^0(\omega)$ can be written as

$$\Pi^0_{\alpha\beta,\gamma\delta}(\omega) = \delta_{\alpha\gamma}\delta_{\beta\delta}\frac{n_\alpha^0 - n_\beta^0}{E_\alpha^0 - E_\beta^0 - \omega}. \tag{5}$$

This fourth rank tensor can be regarded as a matrix acting on the vectors ϕ_{ab}, and thus can be represented as the product

$$\Pi^0(\omega) = \Delta n(\Delta E - \omega I)^{-1}, \tag{6}$$

where Δn and ΔE are diagonal matrices

$$\Delta n_{\alpha\beta,\gamma\delta} = \delta_{\alpha\gamma}\delta_{\beta\delta}(n_\alpha^0 - n_\beta^0),$$

$$\Delta E_{\alpha\beta,\gamma\delta} = \delta_{\alpha\gamma}\delta_{\beta\delta}(E_\alpha^0 - E_\beta^0). \tag{7}$$

The polarization of the interacting system can then be expressed as

$$\Pi(\omega) = \Delta n(\Delta E - \omega I - V\Delta n)^{-1}. \tag{8}$$

Hence the plasmons correspond to charge densities $\delta\rho = \Delta n\phi$ such that

$$(\Delta E - \omega I - V\Delta n)\phi = 0. \tag{9}$$

When the matrix $\Delta E - \Delta nV$ is diagonalized, the polarization has poles at $\omega = \lambda_b$ for each eigenvalue λ_b of $\Delta E - \Delta nV$.

The retarded Green's function $\Pi^R(\omega) = \Pi(\omega + i0^+)$ gives the spectral density function $A(\omega) = -\frac{1}{\pi}\mathrm{Im}\,\Pi^R(\omega)$, which is expressed as

$$A(\omega) = -\Delta n\,\delta(\Delta E - \omega I - V\Delta n). \tag{10}$$

Due to the delta function, $A_{\alpha\beta,\gamma\delta}(\omega)$ is nonzero only for plasmonic frequencies. The only spatial profiles it can display are those of the plasmons $\Delta n_{ab,mn}\phi_{mn}$ with ϕ_{mn} satisfying $(\Delta E - \omega I - V\Delta n)\phi = 0$. In order to plot the plasmon density of states the representation $\delta(\omega - \omega_\alpha) \to \frac{\gamma}{\pi[(\omega-\omega_\alpha)^2+\gamma^2]}$ is used, where γ is chosen to be 0.05 eV. Then the plasmon density of states $\mathrm{tr}\,A(\omega)$ can be written as

$$\mathrm{tr}\,A(\omega) = \sum_\alpha A_\alpha(\omega) = \sum_\alpha A_\alpha \frac{\gamma}{\pi[(\omega - \omega_a)^2 + \gamma^2]}, \tag{11}$$

A_α will be referred to as the strength of the mode

$$A_\alpha = (\phi^\alpha)^T\Delta n\phi^\alpha = \sum_b (\phi^\alpha)^T_{bb}(\Delta n\phi^\alpha)_{bb}, \tag{12}$$

where $\Delta n\phi^\alpha = \delta\rho$ is the charge profile of the mode α. Using Eq. (12), the plasmon is considered to be localized when the major contribution to the sum comes from sites around the impurity. The following discussion of our results is focused on such localized modes. The plasmon density of states $\mathrm{tr}\,A(\omega)$ can be accessed experimentally through scanning tunneling experiments that reveal either direct or inelastic tunneling signatures associated with plasmons or related lifetime effects.[26]

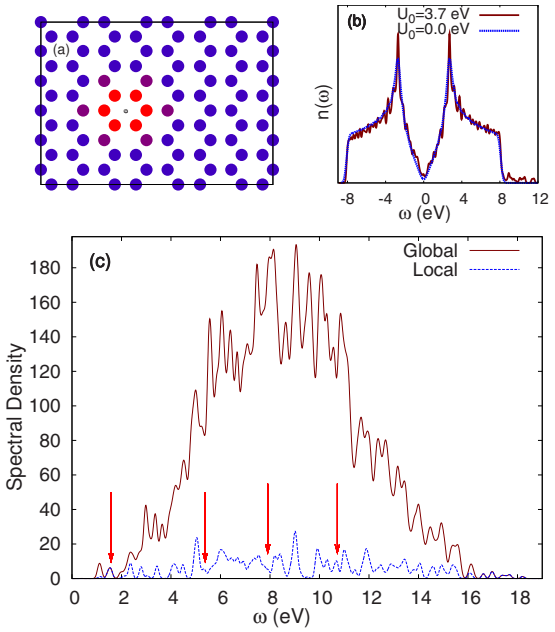

FIG. 1. (Color online) (a) Single impurity on the graphene lattice. Blue (dark gray) corresponds to 0 eV and red (light gray) to 3.7 eV. The black dot indicates the center of the impurity $\mathbf{x}_0$. (b) Single-particle density of states $n(\omega) = -\frac{1}{\pi}\mathrm{Im}\,\mathrm{tr}\,\mathcal{G}^0(\omega) = \Sigma_\beta\delta(\omega - E_\beta^0)$ for pure ($U_0 = 0$) and doped ($U_0 = 3.7$ eV) graphene, both with $\mu = 0$. (c) Spectral density of plasmons in graphene with $\mu = 0$ and $U_0 = 3.7$ eV. "Global" corresponds to the density of states $\mathrm{tr}\,A(\omega) = \Sigma_{all\ \alpha}A_\alpha(\omega)$ and "local" is the spectral density of plasmons localized around the impurity $\mathrm{tr}\,A(\omega) = \Sigma_{local\ \alpha}A_\alpha(\omega)$, here α runs through localized modes only. The arrows indicate the modes shown in Fig. 2.

For the numerical simulation a finite-size realization of the graphene lattice with 96 sites is considered. An impurity affects approximately one hexagon of the honeycomb lattice, as shown in Fig. 1(a). Periodic boundary conditions are used to eliminate the boundary modes. LAPACK routines are used for the numerical diagonalization of H_0 and $\Pi(\omega)$.[27] Due to the overlap of other bands, the tight-binding model is not accurate for energies larger than ~4 eV, therefore our results for plasmons are not accurate for energies larger than ~8 eV.

III. RESULTS

In Fig. 1(b) the single-particle densities of states of pure and impurity doped graphene are shown. They feature two characteristic singularities around ±2.7 eV and a V-shaped dip at the Fermi energy. Please note that there is a tail of states in the doped system beyond the regular bandwidth and also some additional states around $\omega = 0$. In Fig. 1(c) the

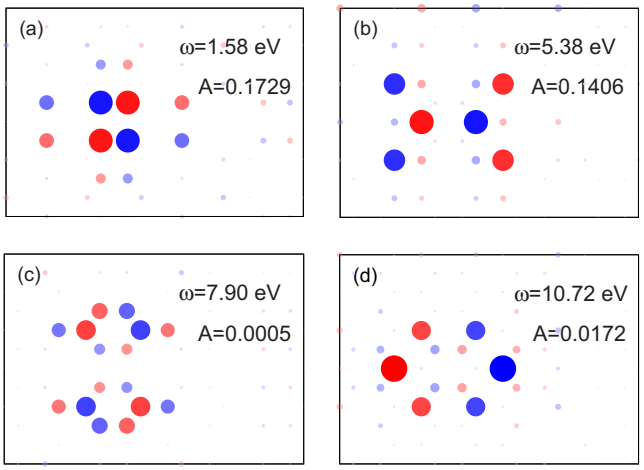

FIG. 2. (Color online) [(a)–(d)] Charge-density profiles of some localized plasmons. Red (light gray) corresponds to negative charge and blue (dark gray) corresponds to positive charges. The plots show the induced charge $(\Delta n \phi^{\alpha})_{bb}$ for the mode α on site b. The frequencies ω and strengths $A_{\alpha}=(\phi^{\alpha})^{T}\Delta n \phi^{\alpha}$ of each mode are also indicated.

spectral density of all plasmon and the spectral density of localized plasmons are shown for $\mu=0$ and $U_0=3.7$ eV. The global density of plasmons can be understood in terms of the single-particle density of states shown in Fig. 1(b). There are very few single-particle states available around $\omega=0$. Then there are two peaks around $\omega=\pm 2.7$ eV. And, at the extrema of the band the single-particle density of states becomes small again. This implies a quadratically increasing spectral density at small ω, a sharp increase around $\omega=2t$, and a small impurity-dominated contribution around $\omega=16$ eV [see Fig. 1(c)]. Localized modes occur throughout the available frequency spectrum. Nonlocal plasmonic modes are most abundant for 5–10 eV because of the larger phase space. The highest energy modes are all localized, i.e., the spectral density of local plasmons equals the total spectral density above 16 eV. This is a consequence of the fact that the high-energy plasmons are excitations from the lowest energy states, which tend to be uniformly spread throughout the lattice, to the tail of highest (localized) single-particle states, thus generating a very localized charge-density profile. The high-energy values for these localized plasmonic modes are set by the very localized nature of the impurity problem. Had the impurity potential range been much larger, on the scale of 10 nm, one would expect those localized plasmonic modes with much smaller energy, on the scale of few electron volts.

In Figs. 2(a)–2(d) the spatial profiles of some selected localized modes are shown. These are representatives for the diversity of localized modes. It is seen that some modes have strong dipole characteristics, whereas others have a strong quadrupole component. This point highlights the importance of resolving the spatial distribution of the induced charge for all possible modes. Previous methods would only be capable of detecting selected few modes with strong dipole moments.[25]

The dependence of the intensity of the localized plasmons (for a fixed impurity potential) on the chemical potential is

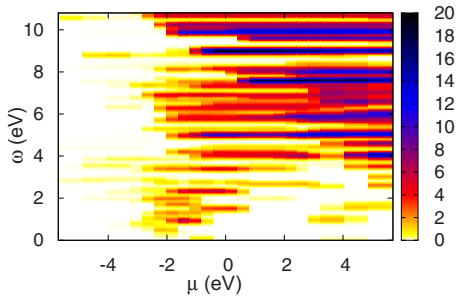

FIG. 3. (Color online) Dependence of the spectral density tr $A(\omega)$ of localized plasmon modes on the chemical potential μ and the frequency ω. The impurity potential is kept fixed at $U_0=3.7$ eV. The spectral density is shown via the color scale (grayscale).

shown in Fig. 3. For larger chemical potentials, more modes are present at lower energies. This is a consequence of the occupation of single-particle states closer to those localized modes at higher energies. When the chemical potential has opposite sign with respect to the impurity potential, there is some spectral density at low energies. These modes stem from the extra single-particle states around $\omega=0$ in doped graphene, seen in Fig. 1(b). This shows that the chemical potential, which can be experimentally controlled through a gate voltage, is an important tuning parameter for achieving certain target modes. A limiting aspect of this property though is that the frequency of the modes does not change very significantly. This happens because the chemical potential does not change the single-particle states but only their occupation. In this sense, the chemical potential does not allow one to control the frequency of localized plasmons but only their existence. As it will be shown below the impurity potential U_0 changes the frequency of the localized modes more effectively. We emphasize that Fig. 3 shows localized plasmonic excitations.[28]

In order to change the frequency of modes, one can vary the impurity potential because it actually affects the single-particle states. Figure 4 shows that for an appropriate change in U_0 the frequency of some localized plasmons can be tuned by about 1 eV. Note also that the impurity potential should be at least 2 eV in order to obtain a significant intensity of localized modes and some modes are strong only within a specific range of the impurity potential (see, e.g., the features

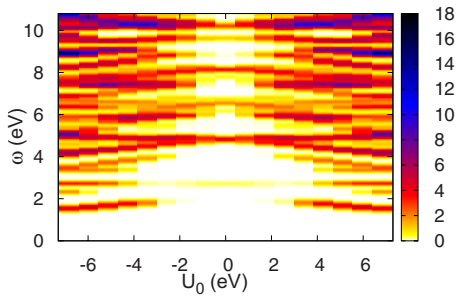

FIG. 4. (Color online) Dependence of the spectral density tr $A(\omega)$ for localized plasmons on the impurity potential magnitude U_0 and on the frequency ω. The chemical potential is kept fixed $\mu=0$. The spectral density is shown via the color scale (grayscale).

at $\omega \sim 6.0$ eV or $\omega \sim 7.5$ eV). The impurity potential considerably changes the spectral intensity of localized plasmons and can therefore be used as a tuning parameter to achieve targeted spectral properties, especially when combined with variations in the chemical potential. This result is in agreement with the fact that the impurity changes the single-particle density of states.[11,12] Another striking feature displayed in this figure is the symmetry of the intensity of the modes with respect to the sign of the impurity potential. This is a consequence of the single-particle spectrum being symmetric relative to $\mu=0$. Since the plasmon involves electrons and holes, its properties do not depend on the sign of the impurity potential.

IV. CONCLUSIONS

We have introduced an RPA approach which resolves the real-space structure of plasmonic modes in graphene. This method was used to show that impurities induce the formation of nanoscale localized plasmonic excitations in graphene sheets. The spatial profile, i.e., dipole vs multipole, of the modes was found to vary strongly with the particular resonance. Furthermore, their frequency and amplitude can be tuned by varying the strength of the impurity potential. We also studied the effect of varying the chemical potential on these modes. It was found that the chemical potential can be used to turn them on and off but it does not affect their frequency. This theoretical study is a step in exploring surface enhancement phenomena in graphene which may prove useful for nanoscale technologies such as molecular sensing.

Note added in proof. Recently, we learned about an experiment related to this topic.[29]

ACKNOWLEDGMENTS

We thank Ming-Chak Ho, Noah Bray-Ali, Yung-Ching Liang, and James Gubernatis for useful conversations. We also acknowledge financial support by the U.S. DOE through Grant No. DE-FG02-05ER46240 and through the BES, UCOP-027 and LDRD funds under Grant No. DE-FG02-06ER46319. The numerical computations were carried out on the USC-HPC cluster.

*rmuniz@usc.edu
†avb@lanl.gov

[1] E. Ozbay, Science **311**, 189 (2006).
[2] A. K. Geim and K. S. Novoselov, Nature Mater. **6**, 183 (2007).
[3] P. R. Wallace, Phys. Rev. **71**, 622 (1947).
[4] K. S. Novoselov, A. K. Geim, S. V. Morozov, D. Jiang, M. I. Katsnelson, I. V. Grigorieva, S. V. Dubonos, and A. A. Firsov, Nature (London) **438**, 197 (2005).
[5] A. H. Castro Neto, F. Guinea, N. M. R. Peres, K. S. Novoselov, and A. K. Geim, Rev. Mod. Phys. **81**, 109 (2009).
[6] V. P. Gusynin and S. G. Sharapov, Phys. Rev. Lett. **95**, 146801 (2005).
[7] M. I. Katsnelson, Eur. Phys. J. B **51**, 157 (2006).
[8] M. Ohishi, M. Shiraishi, R. Nouchi, T. Nozaki, T. Shinjo, and Y. Suzuki, Jpn. J. Appl. Phys., Part 2 **46**, L605 (2007).
[9] I. F. Herbut, V. Juricic, and O. Vafek, Phys. Rev. Lett. **100**, 046403 (2008).
[10] V. W. Brar, Y. Zhang, Y. Yayon, T. Ohta, J. L. McChesney, A. Bostwick, E. Rotenberg, K. Horn, and M. F. Crommie, Appl. Phys. Lett. **91**, 122102 (2007).
[11] C. Bena, Phys. Rev. Lett. **100**, 076601 (2008).
[12] T. O. Wehling, A. V. Balatsky, M. I. Katsnelson, A. I. Lichtenstein, K. Scharnberg, and R. Wiesendanger, Phys. Rev. B **75**, 125425 (2007).
[13] T. O. Wehling, H. P. Dahal, A. I. Lichtenstein, M. I. Katsnelson, H. Manoharan, and A. V. Balatsky, Phys. Rev. B **81**, 085413 (2010).
[14] Y.-W. Tan, Y. Zhang, K. Bolotin, Y. Zhao, S. Adam, E. H. Hwang, S. Das Sarma, H. L. Stormer, and P. Kim, Phys. Rev. Lett. **99**, 246803 (2007).
[15] A. Hill, S. A. Mikhailov, and K. Ziegler, EPL **87**, 27005 (2009).
[16] B. Wunsch, T. Stauber, F. Sols, and F. Guinea, New J. Phys. **8**, 318 (2006).
[17] X.-F. Wang and T. Chakraborty, Phys. Rev. B **75**, 033408 (2007).
[18] E. H. Hwang and S. Das Sarma, Phys. Rev. B **75**, 205418 (2007).
[19] J. Cervenka, K. van de Ruit, and C. F. J. Flipse, Phys. Rev. B **81**, 205403 (2010).
[20] T. Stauber, J. Schliemann, and N. M. R. Peres, Phys. Rev. B **81**, 085409 (2010).
[21] P. K. Pyatkovskiy, J. Phys.: Condens. Matter **21**, 025506 (2009).
[22] M. Jablan, H. Buljan, and M. Soljacic, Phys. Rev. B **80**, 245435 (2009).
[23] V. V. Kresin, Phys. Rep. **220**, 1 (1992); K. D. Bonin and V. V. Kresin, *Electric-Dipole Polarizabilities of Atoms, Molecules and Clusters* (World Scientific, Singapore, 1997).
[24] J. M. McMahon, S. K. Gray, and G. C. Schatz, Phys. Rev. Lett. **103**, 097403 (2009).
[25] I. Grigorenko, S. Haas, and A. F. J. Levi, Phys. Rev. Lett. **97**, 036806 (2006); A. Cassidy, I. Grigorenko, and S. Haas, Phys. Rev. B **77**, 245404 (2008); I. Grigorenko, S. Haas, A. V. Balatsky, and A. F. J. Levi, New J. Phys. **10**, 043017 (2008); R. A. Muniz, S. Haas, A. F. J. Levi, and I. Grigorenko, Phys. Rev. B **80**, 045413 (2009).
[26] V. Brar *et al.*, Phys. Rev. Lett. **104**, 036805 (2010).
[27] E. Anderson, Z. Bai, C. Bischof, L. S. Blackford, J. Demmel, J. Dongarra, J. Du Croz, A. Greenbaum, S. Hammarling, A. McKenney, and D. Sorensen, *LAPACK Users' Guide* (Society for Industrial and Applied Mathematics, Philadelphia, 1999).
[28] There is no contradiction with the well-known fact that the usual bulk plasma frequency for metals depends on the number of electrons in the system. In bulk plasmons almost every electron participates in the excitation while for a localized plasmon there is a definite amount of electrons involved. Adding an extra electron in the system directly affects a bulk-plasmon mode while localized ones are only disturbed through the perturbative interaction.
[29] A. Bostwick, F. Speck, T. Seyller, K. Horn, M. Polini, R. Asgari, A. H. MacDonald, and E. Rotenberg, Science **328**, 999 (2010).